Role of electrons in collision cascades in solids. II. Molecular dynamics

A. Tamm,[1,*] M. Caro,[2] A. Caro,[3] and A. A. Correa[1,*]
[1]*Quantum Simulations Group, Lawrence Livermore National Laboratory, Livermore, California 94550, USA*
[2]*Department of Mechanical Engineering, Virginia Polytechnic Institute, Falls Church, Virginia 22043, USA*
[3]*College of Professional Studies, George Washington University, Ashburn, Virginia 20147, USA*

(Received 14 December 2018; published 7 May 2019)

We present a model for the role of electrons in collision cascades in solids in which the coupling between ions and electrons is calculated using first-principles models and introduced into the classical ion equations of motion using our modified Langevin dynamics [A. Tamm *et al.*, Phys. Rev. Lett. **120**, 185501 (2018)]. This model gives a full picture of the entire collision process, from the ballistic to the thermal phases of a cascade, giving a detailed representation of the energy exchange between ions and electrons until their final thermalization, removing in this way some *ad hoc* assumptions used in the state-of-the-art two-temperature model. This work is separated into two papers: Part I [M. Caro *et al.*, Phys. Rev. B **99**, 174301 (2019)] reports on the *ab initio* methodology used to translate stopping power into the parametrized dissipation function. Part II applies the nonadiabatic ion dynamics using the dissipation functions developed in Part I to specific collision cascade events.

DOI: 10.1103/PhysRevB.99.174302

I. INTRODUCTION

The analysis of the interaction of energetic ions with matter starts with the concept of a primary knock-on atom (PKA). The PKA is the atom of the target that is first hit by the irradiation particle, a neutron, an electron, a γ ray, etc. This atom moves and collides with others in the solid, creating a collision cascade that damages the lattice. This damage has profound effects on the properties of the material. Quantifying this process has been a primary objective of radiation damage theories for decades.

The simplest approach to quantify damage, proposed by Kinchin and Pease (KP) in 1955 [1], has been to consider the energy balance between two-body elastic collisions of hard spheres. The rationale behind this approach has its grounds in the following main assumptions: (i) An atom is displaced from its lattice site if, after a collision, it receives an energy larger than some displacement threshold value E_d; (ii) the arrangement of atoms in the solid is random, i.e., no crystallinity effects. Using the scattering cross section for hard-sphere collisions, the number of displacements N_KP becomes

$$N_\mathrm{KP} = \frac{T_\mathrm{PKA}}{2E_\mathrm{d}}, \tag{1}$$

where T_PKA is the PKA kinetic energy. The KP formula is merely a linear scaling of the available energy for damage in relation to the energy required to produce a single displacement event.

At high PKA energies, this balance needs to be altered because electronic losses become important. Improvements to the KP approach using more elaborate cross sections and consideration of electronic losses led Norgett, Robinson, and Torrens to postulate in 1975 an expression known as the NRT formula [2],

$$N_\mathrm{NRT} = \kappa \frac{(T_\mathrm{PKA} - \eta)}{2E_\mathrm{d}} = \kappa \frac{E_\mathrm{D}}{2E_\mathrm{d}}, \tag{2}$$

where κ is an *efficiency factor*, usually $\sim$0.8, η is a measure of the energy loss to electronic excitations, and T and E_d were defined above. The quantity $E_\mathrm{D} = T_\mathrm{PKA} - \eta$ is known as *damage energy* and is the kinetic energy available to actually displace atoms once the electronic losses are accounted for.

For years, the NRT formula and its related concept, the displacement per atom (dpa), was the workhorse of radiation damage studies and a key concept in nuclear engineering designs until the introduction of large-scale molecular dynamics (MD), the "brute force" solution to the coupled Newton equations for the ions, made its appearance in the 1980's. Within the MD framework, the energy transfer between ions, including chemical bonding and crystalline effects, and from ions to electrons could all be accounted for. For a detailed discussion, see Was [3].

With the increase in computer power and the development of accurate interatomic potentials, MD represents the state-of-the-art calculations of stopping power, range, and microscopic details of the defects produced by radiation damage in solids. One of its main early contributions was to unveil a more elaborate form for the efficiency factor κ in Eq. (2). In fact, many-body effects in the collision cascade, in particular, in the quenching stage, led to a significant reduction of the number of defects produced; the efficiency factor became a function of the energy, with values close to 1 for low PKA energies and decreasing smoothly to about 0.3 for energies in the range of the 10–50 keV for Cu, for example [4]. This result had important consequences on the assessment of the relative damage produced by different sources, e.g., electrons and light ions are more damaging than heavy ions at the same T_PKA because the PKA energy transferred is low.

*Corresponding authors: tamm3@llnl.gov; correaa@llnl.gov

Electronic stopping in the low-energy regime was studied using several theoretical approaches, most notably by Firsov [5] for atomic collisions, and by Lindhard and coworkers in the 1960's [6–9] for projectiles in electron gases. These studies led to the characterization of the electronic stopping S_e as a frictionlike force proportional to the projectile velocity. However, effects of the electronic structure of the target point towards the need for more accurate descriptions of the electronic structure at the low-energy limit [10]. A fully atomistic first-principles calculation of electronic stopping for a wide range of projectile velocities has only recently been possible [11–18]. These advances rely on nonperturbative time-dependent density functional theory (TDDFT) [19].

The computational requirements of the first-principles approach prevent its use in cases where the ion dynamics needs to be followed over much longer time scales, e.g., picoseconds, or to study defect creation. For those cases, the state-of-the-art simulations for the combined system of ion and electron dynamics, in the nonadiabatic picture, is classical MD with empirical potentials for the ions and a continuum heat diffusion equation for the electrons. The two subsystems are connected via electron-ion coupling terms extracted from the *ab initio* theories, in what is termed two-temperature models (TTMs) [20]. For a recent review, see Darkins *et al.* [21].

In its origin, the TTM describes a nonequilibrium state between electrons and ions. Under a radiation damage event, a nonequilibrium state arises between them. Since the time required to establish equilibrium in the electron gas is much shorter than the time required to establish equilibrium between the electrons and the ions, the metal can be considered as composed of two interacting subsystems, one of electrons and another of ions. The thermalization of the hot electron gas with ions is a relatively slow process driven by the electron-phonon interaction. This problem was solved by Ginzburg and Shabanskii in 1955 in the high-temperature limit [22], $T > T_{\text{Debye}}$. The theory of the thermal relaxation of electrons in metals was further extended by Allen [23] in the continuum approximation. It consists of a coupled set of heat diffusion equation, namely,

$$\begin{aligned} C_e \frac{\partial T_e}{\partial t} &= \nabla \cdot (\kappa_e \nabla T_e) - G(T_e - T_\ell) + A, \\ C_\ell \frac{\partial T_\ell}{\partial t} &= \nabla \cdot (\kappa_\ell \nabla T_\ell) - G(T_\ell - T_e), \end{aligned} \tag{3}$$

where C_e and C_ℓ are the specific heat of electrons and ions (lattice), respectively, κ_e and κ_ℓ are their thermal conductivities, T_e and T_ℓ are the electron and ion (lattice) temperatures, G is the electron-phonon (e-ph) coupling, and A is an external source term (e.g., additional laser excitation).

Modern versions of this model replace the second line in Eq. (3) by full MD for the ions, with an added dissipative force on every ion I of the form $\mathbf{f}_I = -\beta_I \mathbf{v}_I$ to account for the e-ph interaction, and a random force term in the framework of Langevin dynamics. The use of Langevin equations with a damping term that is a function of the local electronic density $\beta = \beta(\rho)$ was proposed by one of us in the 1980's [24]. At present, in its most common implementation, the traditional TTM MD assumes β as a piecewise function [21,25,26],

$$\beta_I = \begin{cases} \beta_{S_{\text{e-ph}}} + \beta_{S_e} & (v_I > v_{\text{th}}), \\ \beta_{S_{\text{e-ph}}} & (v_I \leqslant v_{\text{th}}), \end{cases} \tag{4}$$

where S_e and $S_{\text{e-ph}}$ represent the electronic stopping and the e-ph values of the coupling, respectively, both constant values and usually taken from tables in SRIM [27], or theory [28]. The value of v_{th} is an arbitrary threshold parameter, used to adjust the energy absorbed by electrons to match expected results.

This piecewise form reflects the fact that there is no established model to account for the changes in the strength of the electron-ion coupling β as the moving particles change their energy by orders of magnitude.

We recently used time-dependent density functional theory and Ehrenfest forces to calculate the electronic excitations produced by a moving Ni ion in a Ni crystal in the energetic MeV range (electronic stopping power regime), as well as in the thermal meV range (e-ph interaction regime). This results in a picture where ions are still classical but electrons evolve quantum mechanically. We showed that TDDFT not only gives quantitatively accurate values for the stopping power regime [29], but also for the electron-phonon interaction regime when interpreted as a stopping process even for energies in the meV range [30]. Results at high energy compare well to experimental databases of stopping power, and at low energy the e-ph interaction strength determined in this way is very similar to the linear response calculation and experimental measurements. This approach to the e-ph interaction as an electronic stopping process provides the basis for a unified framework to perform classical molecular dynamics of ion-solid interactions with *ab initio*-derived nonadiabatic terms in a wide range of energies.

Additional work on the nonadiabatic equations of motion led us to propose modifications to the Langevin equations that capture in detail the wave-vector $\mathbf{q}$ dependence of the phonon lifetimes, in agreement with quantum mechanics calculations [31]. The modifications are based on a local view of the e-ph interaction obtained as the low-velocity limit of the stopping power of a moving ion.

The model is parameter free, as its components are derived from *ab initio*-type calculations; since it is formulated in real space it is readily extended to the case of nonperiodic systems, e.g., alloys, and it is adequate for large-scale molecular dynamics computer simulations. We also showed how this model removes some oversimplifications of the traditional ionic-damped dynamics commonly used to describe situations beyond the Born-Oppenheimer approximation, such as the inadequate damping of the center-of-mass motion.

More recently, we presented a model that further removes previous limitations, in particular, the different coupling strength for different phonon polarizations while keeping a rigorous statistical mechanics framework and conservation laws [32]. In fact, traditional Langevin dynamics (including traditional TTM MD) relaxes all modes equally, regardless of their wavelength or polarization. We proposed a generalization of Langevin dynamics that captures coupling between collective modes and the bath by introducing spatial correlations in the random forces. This generalization allows modeling the electronic subsystem in a metal as a generalized

Langevin bath endowed with a concept of locality, greatly improving the applicability of the two-temperature model.

The specific form proposed there for the spatial correlations produces a physical wave-vector and polarization dependency of the finite phonon lifetimes in crystals due to e-ph coupling. We show that the resulting model can be used for describing the path to the equilibration of ions and electrons and also as a thermostat to sample the equilibrium canonical ensemble. By extension, the family of models presented there can be applied in general to any dense system, solids, alloys, and dense plasmas.

In this paper, we combine the dissipation function obtained in Part I [33] with the modified Langevin molecular dynamics model reported in Ref. [32], giving a full representation of energy exchanges between ions and electrons in far-from-equilibrium situations as appearing in radiation damage. This is a calculation of the entire process from the collisional to the thermal phases of a cascade, which provides a detailed picture of the energy deposition and exchange between the ion and electron subsystems until their final thermalization.

The paper is organized as follows: In Sec. II we describe the model and simulation methods, by introducing the formalism of our generalized Langevin dynamics to perform molecular dynamics simulations of radiation damage. Next, we summarize the first-principles theory and simulations utilized in Part I of this work to parametrize the nonadiabatic electron dynamics as a dissipative contribution to molecular dynamics. Finally, we describe a family of specific simulations of collision cascades produced by PKA events at different energies in pure Ni and in the NiFeCr alloy. In Sec. III we show the results of the molecular dynamics simulation with emphasis on the nonadiabatic energy transfer between ions and electrons. The discussion in Sec. IV completes the paper.

II. MODEL AND SIMULATIONS

A. Ion-electron interaction model

In the classical MD simulations proposed here, the motion of atoms is governed by a modified Langevin dynamics based on work that we developed in a previous paper [32] and briefly reviewed here. The forces acting on atoms have three contributions: the gradient of the empirical potential, a viscouslike (drag) force, and a random force. To include correlations across particles, the last two terms are given in a tensorial form, making the second term not necessarily antiparallel to the individual velocity. Namely,

$$\begin{aligned}\mathbf{f}_I(\{\mathbf{r}_K\},\{\mathbf{v}_K\},t)&=-\nabla_I U_{\rm adiab}(\{\mathbf{r}_K\})-\sum_J \mathsf{B}_{IJ}(\{\mathbf{r}_K\})\mathbf{v}_J\\&\quad+\sum_J \mathsf{W}_{IJ}(\{\mathbf{r_I}\})\boldsymbol{\xi}_J.\end{aligned}\tag{5}$$

The first term describes the adiabatic forces, which derives from a conservative potential $U_{\rm adiab}$. In the rest of the paper we use the formalism of the embedded atom model (EAM potential) [34]. The second and third terms are the nonadiabatic forces $\mathbf{f}_I^{\rm e\text{-}i}$ arising from the interaction of the ions with an electronic reservoir (e-i), assumed to be respectively linear with the velocities (second term, drag) and stochastic (third term, fluctuations). The matrices B and W, which are functions of positions alone, describe the spatial correlations between particles, and are related through the fluctuation-dissipation theorem,

$$\mathsf{B}_{IJ}=\sum_K \mathsf{W}_{IK}\mathsf{W}_{JK}^{\rm T}.\tag{6}$$

The independent random variables (vectors) $\boldsymbol{\xi}_J$ in Eq. (5) are white noise generated by a thermal bath at local temperature $T_{\rm e}$. These random variables are then combined by the matrix W, resulting in spatially correlated forces on individual ions, defined as

$$\mathsf{W}_{IJ}=\begin{cases}-\alpha_J(\bar\rho_J)\frac{\rho_I(r_{IJ})}{\bar\rho_J}\mathbf{e}_{IJ}\otimes\mathbf{e}_{IJ} & (I\neq J),\\ \alpha_I(\bar\rho_I)\sum_{K\neq I}\frac{\rho_K(r_{IK})}{\bar\rho_I}\mathbf{e}_{IK}\otimes\mathbf{e}_{IK} & (I=J),\end{cases}\tag{7}$$

where $\mathbf{e}_{IJ}$ is the unit vector joining atoms I and J. The coupling function $\alpha_I(\bar\rho_I)$ includes the physics of the coupling strength between specific ion types and electrons. The projection on $\mathbf{e}_{IJ}$ ensured pair radial forces, removing local torques.

We introduced the concept of locality via a weighting function across neighbors, represented by decreasing radial functions ρ_I associated with each ion I. In the current study, the atomic electron density is used for the weighting functions so that the bath effects of an atom at position $\mathbf{r}_J$ on an atom at position $\mathbf{r}_I$ will decrease with the distance between ions r_{IJ}.

With this definition of the random forces, the net force and torque of the system is zero, a condition that we proved necessary to describe phonon lifetimes with the correct wave-vector and polarization dependence [32]. This algorithm defines a correlation between the components of the random forces on individual particles as well as across particles. Correspondingly, the set of *all* associated friction forces is a linear function in the set of *all* the velocities. For instance, the friction (drag) force on a specific particle can depend on the velocity of a close neighbor.

Here, a modification to the initial model [32] is introduced by making the electron-ion coupling strength $\alpha(\bar\rho)$ a function of the local density where the moving atom is located, similarly as originally proposed by Caro and Victoria [24]. The nominal site density is calculated as a superposition of contributions from neighboring atoms, $\bar\rho_I=\sum_{J\neq I}\rho_J(r_{IJ})$; in turn, they are approximated by using spherical atomic densities obtained by solving the isolated atomic problem (for each atomic species), as described in Ref. [33]. For a given configuration, the strength of the random force and the friction linear operator is indirectly (through the density construction) a function of the position.

The only free parameter in this formulation is the coupling factor $\alpha(\bar\rho)$, which is species dependent in this theory. This function has to be defined in the relevant range of $\bar\rho$ explored by the system; for a bulk calculation the range extends from a minimum at the vacancy electronic density ($\sim 0.05e/\text{Å}^3$), all the way to the electronic densities defined by the closest binary collision expected to occur during the simulation ($\sim 2.0e/\text{Å}^3$). Such a function is obtained by fitting TDDFT data, as described in the accompanying paper [33].

Once we interpret the electronic subsystem as a thermodynamic bath endowed with the concept of locality, it is natural to think of it as a spatially modulated heat

reservoir. The simplest realization of this heat reservoir is one in which heat fluxes and temperature gradients arise. Using a bulk electron thermal conductivity and Fourier law, we can relate the gradients to the fluxes. The heat bath composed of electrons is thus modeled with a heat diffusion equation to be solved simultaneously with MD for the atoms, where the electronic heat capacity (C_e) and heat conduction (κ_e) define the evolution of the temperature within the electronic system, Eq. (8). The energy exchange between the electronic and ionic system is controlled by a source term ($Q_{e\text{-}i}$),

$$C_e \frac{\partial T_e}{\partial t} = \nabla \cdot (\kappa_e \nabla T_e) + Q_{e\text{-}i}. \tag{8}$$

The local source term $Q_{e\text{-}i}(\mathbf{r}) = -\sum_I \mathbf{f}_I^{e\text{-}i} \cdot \mathbf{v}_I \delta(\mathbf{r} - \mathbf{r}_I)$ in the diffusion equation couples the continuum electronic system to the atomic system (ions), and is the counterpart of the second and third terms in Eq. (5). This equation is also subject to boundary conditions that are not addressed in this paper.

The model is fully defined by providing, for each element, a spherical atomic density $\rho_I(r)$ (which we regard as given here) and a coupling function $\alpha_I(\bar{\rho})$ as a function of the environment density. The coupling function $\alpha(\bar{\rho})$ defines the overall magnitude of the random forces, and therefore, also of the friction forces. The sought-after function $\alpha(\bar{\rho})$ must satisfy two main requirements. First, that the dynamical model reproduces the e-ph coupling strength for a crystalline phase and, second, that the electronic stopping power is recovered under ballistic, e.g., channeling conditions. The e-ph coupling can be obtained by either using first-order perturbation theory [35] or by doing TDDFT simulations in the e-ph regime [30], while the electronic stopping for channeling can be acquired by first-principles TDDFT calculations [33].

This generalization of classical molecular dynamics with e-ph coupling (termed here EPH-MD) provides a single framework to fully describe the dissipative process in both the high-energy stopping and the thermalization regimes, which is the main goal of this series of papers.

B. Model parameters

To apply the model in simulations of collision damage cascades in pure Ni and concentrated solid solutions such as NiFeCr [36], two functions are required for the former and six for the latter case]one density function $\rho(r)$ and one density-dependent coupling function $\alpha(\bar{\rho})$ for each element]. The reader is referred to the accompanying paper for the determination of these functions [33], which are reproduced here for clarity, in Fig. 1 for the densities, and in Fig. 2 for $\alpha(\bar{\rho})$. It is important to note here that the present parametrization of the model is limited to PKA energies below ∼100 keV because the first-principles calculations in Ref. [33] were done with only up to $3p$ explicit semicore states, preventing the excitation of deeper core levels at higher PKA energies.

The classical-continuum model has been implemented as an extension (*fix*) for the LAMMPS MD code [38] and is released as an open-source code at the LLNL software repository [39]. Similarly to the close-range-corrected ion-ion (EAM) empirical potential, the electron-ion part of the model is supplied with tabulated functions $\rho(r)$ and $\alpha(\bar{\rho})$ for individual elements.

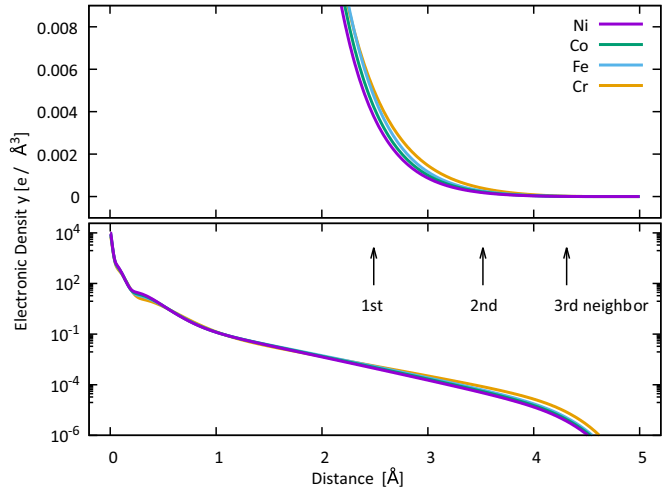

FIG. 1. Electronic density as a function of distance to the nucleus calculated for isolated atoms in vacuum, an approximation we adopt to the actual electronic densities along the trajectory of projectiles in our model. Arrows indicate distances for neighbors in the fcc lattice. For clarity, the lower panel is plotted in logarithmic scale.

The electronic subsystem is integrated with the finite-difference method (FDM), using the midpoint forward-propagation rule in a coarse regular spatial grid where the time step is selected so that the numerical stability criteria are met [40]. This means that depending on the electronic heat capacity and conductivity, there may be many steps within the electronic system between each ionic integration step.

Because in our model the electron-ion interaction is defined with fast decaying spherical functions (Fig. 1), the size

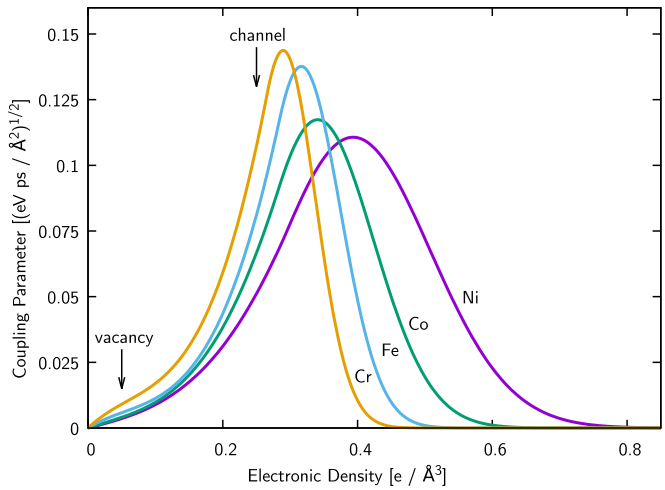

FIG. 2. Dissipation functions for each element of interest $\alpha_{Ni}(\bar{\rho})$, $\alpha_{Co}(\bar{\rho})$, $\alpha_{Fe}(\bar{\rho})$, $\alpha_{Cr}(\bar{\rho})$ that parametrizes W_{IJ} and B_{IJ} in Eq. (5). These functions univocally relate the unperturbed electronic density to dissipation, and represent a simplification to the *ab initio* relationship such as that given in Ref. [37]. Arrows indicate the density at a vacant site and at the center of a ⟨001⟩ channel. Higher densities are explored by close collision events. The coupling is not necessarily an increasing function of the density, because in a real material higher densities are also associated with core atomic-level excitations which are hard to produce by ion motion.

of the atom neighbor list is controlled by a rather small radial cutoff (5 Å); the electronic grid size is independent of ions, implying that if the conductivity is high, a sparse grid or even single point can be used, since electronic temperature equalizes quickly.

The maximum grid size for the heat diffusion equation is set by the maximum value of the heat conductivity, but on the other hand, there exists a possible physical limit for the smallest grid size given by the electronic mean free path. Contrary to standard two-temperature MD, the grid size is independent of the ionic problem since the ionic temperature does not appear explicitly in our equations [see Eq. (12) in Ref. [25] and below Eq. (4) in Ref. [41]].

C. EPH-MD simulations

Two sets of simulations were run to investigate the nonadiabatic aspects of radiation damage, one with the dissipation forces alone, to compare our EPH-MD model with other models in the literature, and one with both dissipation and random forces acting simultaneously, to study the dynamics of the energy exchange between electrons and ions.

In the first type of simulations, we aim at comparing our model to the standard TTM Langevin model, in which the friction force is a constant times the velocity of the ion, $\mathbf{f}^{\text{e-i}} = -\beta\mathbf{v}$, with β having two values, one corresponding to the e-ph interaction for low velocities, $\beta_{\text{e-ph}}$, and one corresponding to the electronic stopping power regime for high ion velocities, $\beta_{S_{\text{e-ph}}} + \beta_{S_e}$ [see Eq. (4) and Eqs. (2) and (3) in Ref. [25]].

For a meaningful one-to-one model comparison, the trajectories of every atom in a collision cascade are the same; to this end, the simulations were run in the microcanonical ensemble, i.e., with no dissipation forces, but the work done by the dissipation forces was recorded at each time step as if they were acting. We ran 20 collision cascades at three different PKA energies for Ni (0.1, 1, and 10 keV), up to 10 ps. In the simulations, the lattice was initially at rest and one atom in the center of the box of a $32 \times 32 \times 32$ conventional fcc supercell was given a velocity in a random direction, matching the selected PKA energies. In the case of standard Langevin we used a constant coupling function given by SRIM for electronic stopping of Ni in Ni from Ref. [27], as is customary done [26]. For the test of our model, we used the functions determined in Ref. [33].

The second set of simulations was run for collision damage events for various PKA energies, with both friction and random forces active, as well as the heat equation in the electronic subsystem. The heat equation is treated at the level of single-cell approximation [i.e., we solve Eq. (8) with the first term on the right-hand side equal to zero], which is equivalent to assuming a uniform electronic temperature in the supercell. This simplification is justified by the significantly higher heat conductivity of electrons compared to the lattice and the small sample size ($L = 11$ nm). We used a constant temperature heat capacity with a value of 3.5×10^{-6} eV/(Å^3 K), representative of the value in the range of representative temperatures $T_e = 300$–1000 K [42]. As in the previous case, the lattice is initially at rest as well as electrons at zero temperature; next, an atom in the center of the box is given an initial velocity corresponding to the PKA energy in a random direction. For each energy, ten simulations with different initial conditions are carried out for statistics.

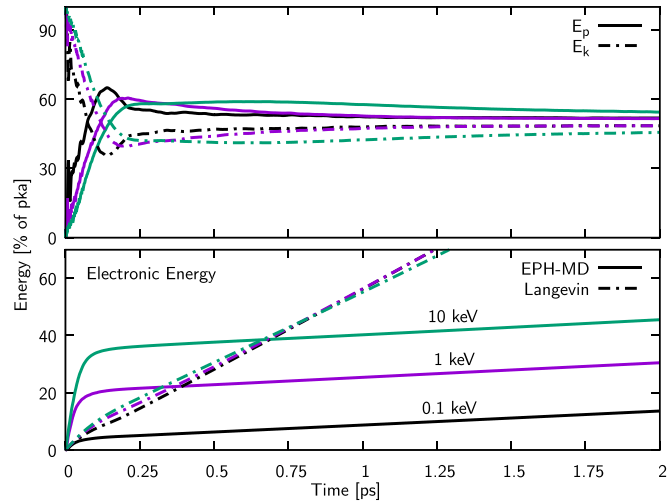

FIG. 3. Upper panel: Ion-kinetic E_k (dashed line) and potential, relative to equilibrium, $E_p = U_{\text{adiab}} - U^0_{\text{adiab}}$ (solid line) of the system as a function of time at three PKA energies 0.1, 1.0, and 10.0 keV along NVE trajectories. Lower panel: Energy deposition to the electronic system in the early stages of collision cascade PKA energies for both models, traditional Langevin (TTM-MD) and EPH-MD (this work). The energy transfer to electrons is obtained by integration of the friction forces, which is calculated but not applied in the integration of the equations of motion. (Solid lines are obtained with our model and dashed lines with standard Langevin with S_e taken from SRIM table energies [27] and no threshold velocity.)

For the first term on the right-hand side of Eq. (5), we used the modified EAM-type potential for Ni by Stoller *et al.* [43], which reproduces the universal Ziegler-Biersack-Littmark (ZBL) repulsive potential at short distances, and was modified to match with DFT energies in the intermediate range.

Finally, we also studied a concentrated solid solution, namely, NiFeCr, with the EPH-MD model parametrized from TDDFT data [33], and an EAM-type potential based on Bonny's [44] and modified by us previously [45] to reproduce DFT data at short distances.

III. RESULTS AND DISCUSSION

A. Early stage of collision cascade in Ni

1. Comparison of dissipation terms

We report here the first type of simulations described above, i.e., microcanonical (NVE) trajectory with the evaluation of dissipative forces according to both traditional Langevin and EPH-MD models. The time evolution of the atomic kinetic and potential energy is shown in the upper panel of Fig. 3. These two energy terms reach the same value at about 0.2 ps, which nominally corresponds to the end of the ballistic phase, after which the system slowly evolves into equilibrium (and approximate equipartition between kinetic and potential energy).

The lower panel of Fig. 3 shows the (virtual) work done by the dissipative forces on all atoms for both models. As

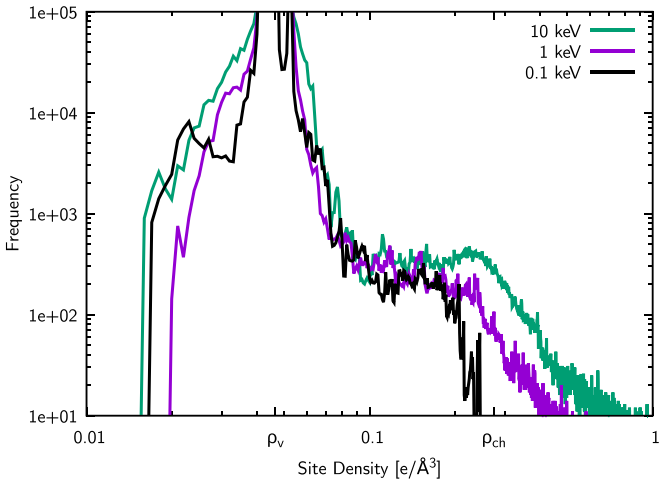

FIG. 4. Histogram of host electronic densities that a Ni projectile with different initial energies explores during a collision cascade event. This gives the range in which the coupling function α needs to be modeled (Fig. 2). For reference, ρ_v and ρ_{ch} mark typical valence (site) and channel densities, respectively. Only briefly after the PKA event and at $T_{PKA} > 1$ keV a few ions can explore channel ("ch") conditions which are associated with maximal electron-ion coupling α (Fig. 2), in turn producing high electronic dissipation at subpicosecond times (Fig. 3).

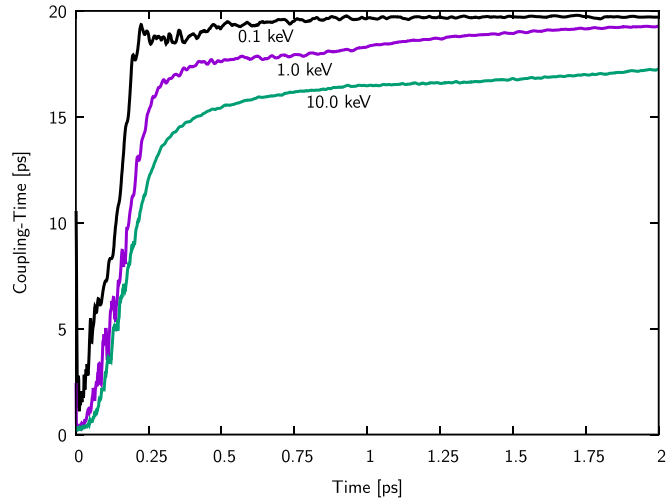

FIG. 5. Effective instantaneous relaxation time τ as the cascade progresses for three PKA energies, 0.1, 1.0, and 10 keV. Given an NVE trajectory, the instantaneous relaxation time was estimated globally as $\tau = 2E_k/(dE_e/dt)$. A lower value of τ means a higher effective coupling.

expected, the traditional Langevin viscous damping removes the same fraction of energy linearly with time at a (large) rate determined by the electronic stopping power, independently of the PKA energy. It clearly demonstrates the need to set an arbitrary energy or velocity threshold [v_{th} in Eq. (4)] for this term, or otherwise all the energy would rapidly transfer to the electrons. For example, in the work by Zarkadoula *et al.* a fixed value around 31–54 Å/ps was chosen for similar applications (see Table I in Ref. [26]).

In contrast, the EPH-MD model presented here clearly shows two distinct regimes, one of strong coupling, when atoms in the cascade are in ballistic trajectories undergoing close collisions and dissipating significant amounts of energy, and another, the e-ph regime, with smaller coupling. The transition is generated by the environment dependence of the coupling function α, via $\bar{\rho}$: It is smooth, it happens at a small fraction of a ps, and it depends on the PKA energy because higher energies imply higher explored values of $\bar{\rho}$. This model captures this transition with a continuous model and gives quantitative information about this process. Our tests show that it is unlikely that a single threshold value in the model of Eq. (4) can match the energy balance of Fig. 3 (lower panel, solid lines) in this range of PKA energies.

As an illustration of these features of the EPH-MD model, Fig. 4 shows the host densities that a projectile explores during a cascade event. At low energy (0.2 keV) the projectile explores host densities equal to or below those corresponding to center of the ⟨001⟩ channel; the main contribution to dissipation comes from the low-density region of $\alpha(\bar{\rho})$ on Fig. 2, while at 10 keV the whole range of densities of the coupling function $\alpha(\bar{\rho})$ is sampled.

Since the intensity of the electron-ion coupling is environment dependent, it is also natural to assume that the relaxation time of ionic energy to the electronic system is also *effectively* time dependent. The effective relaxation time, defined as the rate of energy loss of the ionic system, is illustrated in Fig. 5.

2. *Collision cascades of Ni in Ni: Full dynamic evolution*

We report here the second set of simulations of collision damage events for Ni projectiles in a Ni target at various PKA energies, with both friction and random forces active, as well as the heat equation in the electronic subsystem.

The fraction of the PKA energy transferred to electrons versus time for collision cascade simulations for a Ni projectile into a Ni target is shown on Fig. 6, while the temperature of both subsystems versus time is shown in Fig. 7. Figures 5–7 are the main results of this work.

The electronic energy evolution clearly shows the two expected regimes of collision cascades. First, in the early ballistic stage (lasting a fraction of a picosecond), a regime with a high electronic stopping power is responsible for a transfer from atoms to electrons of up to 35% of the PKA energy for $T_{PKA} = 50$ keV. This effect is at the basis of the *damage energy* concept: the fraction of the PKA energy that is actually available to damage the lattice. An equilibration stage follows, originating in the inverse process: electrons transferring excess energy back to atoms; in the computational model, this is achieved by the random force term of the modified Langevin dynamics [third term in Eq. (5)].

Figure 7 shows the time evolution of temperatures in both electrons and ions. For the lattice temperature, we see the transition from the ballistic to thermal stage at ∼0.1 ps, as mentioned when discussing Fig. 3. This figure clearly shows that the electronic subsystem transition from an energy absorber to energy emitter occurs at the same time when the ions evolve from ballistic to thermal stages.

The combined electron-and-ion system conserves energy, and since in the initial state all the energy is in the PKA

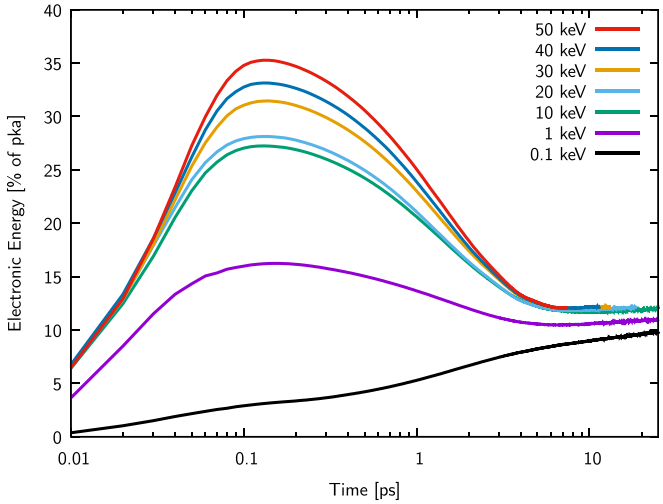

FIG. 6. Fraction of energy, initially in a PKA Ni projectile, transferred to the electronic system as a function of time during a collision cascade event at various PKA energies. The maximum value is interpreted as the energy loss to electronic excitations [η in Eq. (2)] in a realistic cascade (large open system) and plotted in Fig. 8.

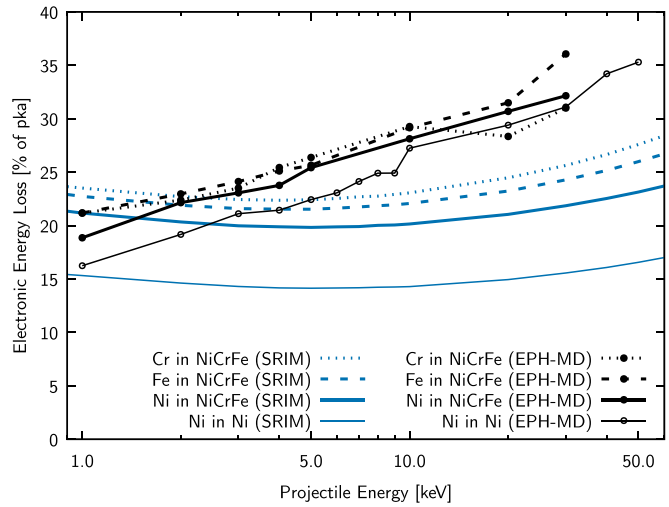

FIG. 8. Fraction of energy deposited into the electronic system as predicted by our EPH-MD model (black points) (maximum values in Figs. 6 and 9) and by SRIM (blue curves). The results are shown for a pure Ni projectile in pure Ni (thin curve) and Cr, Fe, and Ni in a NiFeCr random alloy (thick curves).

motion, the final equilibrium temperature is directly related to the PKA energy, as shown in Fig. 7.

Figure 7 also shows that the thermal equilibration stage can last more than 25 ps, which is in agreement with our previous work on the lifetimes of phonons due to the e-ph interaction [32]. Note that the present simulations are done for a small closed system, with no thermal gradients in the electronic subsystem and no boundary sink terms for simplicity. For larger samples, with the full heat diffusion equation for electrons, a faster thermal equilibration is expected.

From Fig. 6 we extract the highest percentages of energy deposited into the electronic system and plot them as a function of projectile energy, shown in Fig. 8. This quantity can be interpreted as η in the NRT theory [Eq. (2)].

SRIM simulations of Ni projectiles in Ni are also shown for comparison. Figure 8 shows that our model predicts a significantly larger energy loss than SRIM, an effect probably due to the fact that SRIM assumes a constant scalar linear stopping power in the projectile energy range from 1 to 130 keV.

Finally, we ran the 10-keV cascade with TTM MD with the SRIM stopping power value and our EPH-MD to compare the defect production with both models. On average, in our model, the number of Frenkel pairs at the end of the 50-ps simulation was 18.7 [3.2 standard deviation (SD)] and with TTM MD 26.3 (4.7 SD). Although these values cannot be compared directly to experiments (due to small simulations and unrealistic boundary conditions), the results clearly show the difference between the two models having a significant p value in Welch's t-test ($p = 0.0007$).

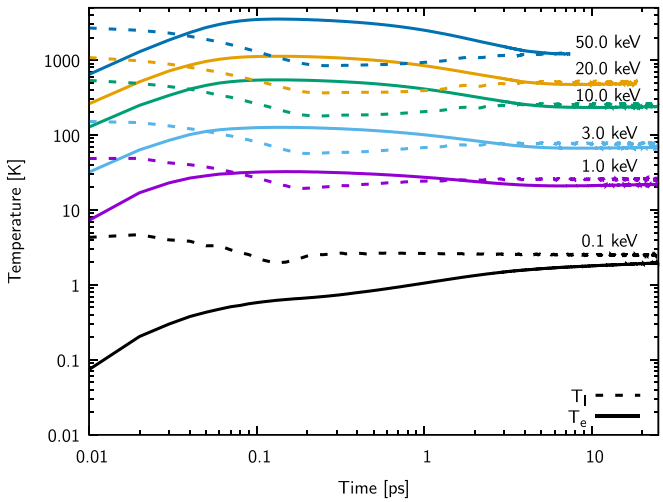

FIG. 7. Evolution of electronic T_e (solid curves) and lattice T_l (dashed curves) temperatures during collision cascade events initiated by Ni projectiles (PKA) at different energies. Note that the use of the expression "lattice temperature" is not well defined during the ballistic regime (before kinetic-potential crossing in Fig. 3).

B. Collision cascades of Ni, Fe, and Cr in a NiFeCr random alloy

In the accompanying paper, we report model parametrization for the four elements in the NiCoFeCr concentrated solid solution. However, there are no classical potentials U_{adiab} of the EAM type to perform MD simulations for such a quaternary system including Co. Therefore, we applied our EPH-MD model to study collision cascades in the ternary NiFeCr random alloy, which has an EAM potential available in the literature [44], and serves to display the ability of the EPH-MD model to describe alloys.

The results for cascades initiated by each of the three different elements are shown on Fig. 9. The same trends as for pure Ni are also visible in the alloy case, where the initial collision cascade regime transitions smoothly into the e-ph regime. No significant differences are observed for different elements used as PKAs. Although the electron-ion coupling

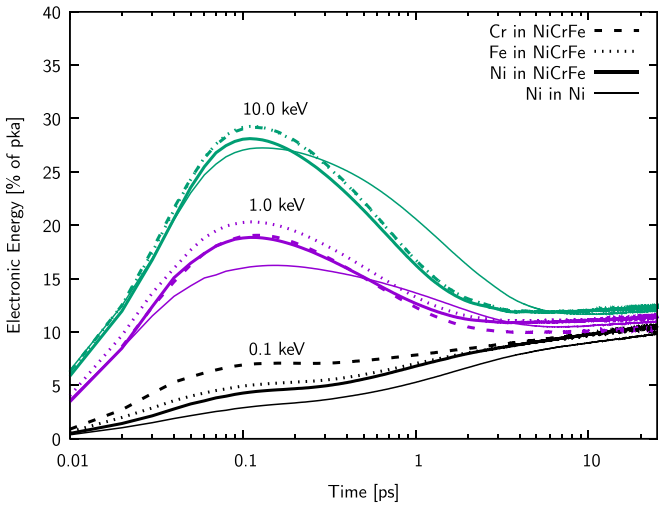

FIG. 9. Energy transfer by different projectiles into the electronic system as a function of time during a collision cascade event at various PKA energies. The maxima are interpreted as energy losses to electronic excitations [η in Eq. (2)] and are plotted in Fig. 8.

functions for different species are slightly different, the energy deposition curves for the element types studied are quite similar, reflecting the fact that the role of the primary knock-on atom in a collision cascade at these low energies is not relevant because the energy is rapidly distributed among all atoms after a few collisions. In other words, at low energies, the result of a collision cascade is an average of the alloy properties, regardless of the chemical identity of the PKA.

In Fig. 8 we compare the cascade simulation results with similar SRIM calculations. The results are qualitatively similar to those of the pure Ni case, namely, that SRIM reflects a significantly smaller energy dependence in this energy range.

IV. CONCLUSION

This work presents a study of the dynamics of energy exchanges between ions and electrons in the cascade collision process that follows the interaction of an energetic ion with a metallic target. The model is based on a modified Langevin dynamics for the ions that we published recently [32], which takes into account the complex coupling to electrons. Additionally, due to the explicit dependence on local density, the model simultaneously captures the strong coupling corresponding to the electronic stopping power regime, and the weak coupling corresponding the e-ph interaction regime. This last regime is captured with all its complexity, in particular, with the dependence of phonon lifetimes on wave vector and polarization.

The parametrization of the model is presented in the accompanying paper [33], where first-principles time-dependent density functional theory is used to provide electronic stopping and electron phonon interactions. This information is used to construct dissipation functions readily usable in classical MD simulations.

The model has been implemented as an extension for LAMMPS [38] and is released as an open-source code at the LLNL GITHUB page [39]. The computational cost of this model is about 50% higher than the standard TTM MD (1.5 times slower), mainly due to the need to calculate the nontrivial extra dissipative force from ion positions and velocities.

The simulations reported here present a unified picture of a collision process, starting with an energetic ion, the PKA, and ending with a system with both electrons and ions in thermal equilibrium. Between these initial and final states, a complex energy exchange process occurs, starting with the kinetic energy of ions going to the electrons, followed by the excess electronic energy of electrons going back to the ions. While this picture was qualitatively known, this model shows quantitatively and with very few free parameters the precise nature of this interaction.

These results represent a step further in the description of damage processes, in particular, it helps remove the arbitrariness in the election of a cutoff energy (velocity threshold) range for the stopping power regime in the state-of-the-art two-temperature models, providing a quantitative estimate of the damage energy that is left available to damage the lattice. It also provides a means to describe cases of high electronic excitations, such as those in swift heavy ion tracks. Finally, this model also gives an assessment of the accuracy of the SRIM code.

ACKNOWLEDGMENTS

Work performed at the Energy Dissipation to Defect Evolution Center, an Energy Frontier Research Center funded by the US Department of Energy (Award No. 2014ORNL1026). Computing support for this work came from the Lawrence Livermore National Laboratory Institutional Computing Grand Challenge program. Work by A.T. and A.A.C. was performed under the auspices of the US Department of Energy by Lawrence Livermore National Laboratory under Contract No. DE-AC52-07NA27344.

[1] G. H. Kinchin and R. S. Pease, Rep. Prog. Phys. **18**, 1 (1955).
[2] M. J. Norgett, M. T. Robinson, and I. M. Torrens, Nucl. Eng. Des. **33**, 50 (1975).
[3] G. S. Was, *Fundamentals of Radiation Materials Science: Metals and Alloys* (Springer, Berlin, 2018).
[4] S. J. Zinkle and B. N. Singh, J. Nucl. Mater. **199**, 2287 (1993).
[5] O. B. Firsov, Zh. Eksp. Theor. Fiz. **36**, 1517 (1959).
[6] J. Lindhard and M. Scharff, Phys. Rev. **124**, 128 (1961).
[7] J. Lindhard, V. Nielsen, M. Scharff, and P. V. Thomsen, Mat. Fys. Medd. Dan. Vid. Selsk. **33**, 10 (1963).
[8] J. Lindhard, M. Scharff, and H. E. Schiott, Mat. Fys. Medd. Dan. Vid. Selsk. **33**, 1 (1963).

[9] J. Lindhard, V. Nielsen, and M. Scharff, Mat. Fys. Medd. Dan. Vid. Selsk. **36**, 10 (1968).

[10] J. H. Ormrod and H. E. Duckworth, Can. J. Phys. **41**, 1424 (1963).

[11] A. A. Correa, J. Kohanoff, E. Artacho, D. Sánchez-Portal, and A. Caro, Phys. Rev. Lett. **108**, 213201 (2012).

[12] Y. Miyamoto and H. Zhang, Phys. Rev. B **77**, 161402(R) (2008).

[13] S. Bubin, B. Wang, S. Pantelides, and K. Varga, Phys. Rev. B **85**, 235435 (2012).

[14] A. V. Krasheninnikov, Y. Miyamoto, and D. Tománek, Phys. Rev. Lett. **99**, 016104 (2007).

[15] J. M. Pruneda, D. Sánchez-Portal, A. Arnau, J. I. Juaristi, and E. Artacho, Phys. Rev. Lett. **99**, 235501 (2007).

[16] M. A. Zeb, J. Kohanoff, D. Sánchez-Portal, A. Arnau, J. I. Juaristi, and E. Artacho, Phys. Rev. Lett. **108**, 225504 (2012).

[17] I. Tavernelli, M.-P. Gaigeot, R. Vuilleumier, C. Stia, M.-A. Hervé du Penhoat, and M.-F. Politis, Chem. Phys. Chem. **9**, 2099 (2008).

[18] A. Ojanperä, A. V. Krasheninnikov, and M. Puska, Phys. Rev. B **89**, 035120 (2014).

[19] E. Runge and E. K. U. Gross, Phys. Rev. Lett. **52**, 997 (1984).

[20] D. M. Duffy, S. Khakshouri, and A. M. Rutherford, Nucl. Instrum. Methods Phys. Res., Sect. B **267**, 3050 (2009).

[21] R. Darkins and D. M. Duffy, Comput. Mater. Sci. **147**, 145 (2018).

[22] V. L. Ginzburg and V. P. Shabanskii, Dokl. Akad. Nauk SSSR **100**, 445 (1955).

[23] P. B. Allen, Phys. Rev. Lett. **59**, 1460 (1987).

[24] A. Caro and M. Victoria, Phys. Rev. A **40**, 2287 (1989).

[25] D. M. Duffy and A. M. Rutherford, J. Phys.: Condens. Matter **19**, 016207 (2007).

[26] E. Zarkadoula, G. Samolyuk, and W. J. Weber, AIP Adv. **8**, 015121 (2018) .

[27] J. F. Ziegler, J. P. Biersack, U. Littmark, and H. H. Anderson, *The Stopping and Ranges of Ions in Matter* (Pergamon, Oxford, UK, 1985).

[28] G. D. Samolyuk, L. K. Béland, G. M. Stocks, and R. E. Stoller, J. Phys.: Condens. Matter **28**, 175501 (2016).

[29] R. Ullah, E. Artacho, and A. A. Correa, Phys. Rev. Lett. **121**, 116401 (2018).

[30] A. Caro, A. A. Correa, A. Tamm, G. D. Samolyuk, and G. M. Stocks, Phys. Rev. B **92**, 144309 (2015).

[31] A. Tamm, G. Samolyuk, A. A. Correa, M. Klintenberg, A. Aabloo, and A. Caro, Phys. Rev. B **94**, 024305 (2016).

[32] A. Tamm, M. Caro, A. Caro, G. Samolyuk, M. Klintenberg, and A. A. Correa, Phys. Rev. Lett. **120**, 185501 (2018).

[33] M. Caro, A. Tamm, A. A. Correa, and A. Caro, Phys. Rev. B **99**, 174301 (2019).

[34] M. S. Daw and M. I. Baskes, Phys. Rev. B **29**, 6443 (1984).

[35] G. D. Gaspari and B. L. Gyorffy, Phys. Rev. Lett. **28**, 801 (1972).

[36] Y. Zhang, G. M. Stocks, K. Jin, C. Lu, H. Bei, B. C. Sales, L. Wang, L. K. Beland, R. E. Stoller, G. D. Samolyuk, M. Caro, A. Caro, and W. J. Weber, Nat. Commun. **6**, 8736 (2015).

[37] M. Caro, A. Tamm, A. A. Correa, and A. Caro, J. Nucl. Mater. **507**, 258 (2018).

[38] S. Plimpton, J. Comput. Phys. **117**, 1 (1995).

[39] LAMMPS: Large-scale Atomic/Molecular massively Parallel Simulator is a classical molecular dynamics code http://lammps.sandia.gov, utilized here in combination with USER-EPH, a custom developed package for parametrized electron-phonon coupling http://github.com/LLNL/USER-EPH .

[40] W. H. Press, S. A. Teukolsky, W. T. Vetterling, and B. P. Flannery, *Numerical Recipes: The Art of Scientific Computing*, 3rd ed. (Cambridge University Press, New York, 2007).

[41] D. S. Ivanov and L. V. Zhigilei, Phys. Rev. B **68**, 064114 (2003).

[42] Z. Lin, L. V. Zhigilei, and V. Celli, Phys. Rev. B **77**, 075133 (2008).

[43] R. E. Stoller, A. Tamm, L. K. Béland, G. D. Samolyuk, G. M. Stocks, A. Caro, L. V. Slipchenko, Y. N. Osetsky, A. Aabloo, M. Klintenberg, and Y. Wang, J. Chem. Theory Comput. **12**, 2871 (2016).

[44] G. Bonny, D. Terentyev, R. C. Pasianot, S. Poncé, and A. Bakaev, Model. Simul. Mater. Sci. Eng. **19**, 085008 (2011).

[45] L. K. Béland, A. Tamm, S. Mu, G. D. D. Samolyuk, Y. N. N. Osetsky, A. Aabloo, M. Klintenberg, A. Caro, and R. E. E. Stoller, Comput. Phys. Commun. **219**, 11 (2017).